The stability and melting of aragonite: an experimental and thermodynamic model for carbonated eclogites in the mantle

Sutao Zhao[a,b,*], Erwin Schettino[a], Marco Merlini[a] and Stefano Poli[a]

a. Dipartimento di Scienze della Terra, Università degli Studi di Milano, Via Botticelli 23, Milano 20133, Italy;

b. Institute of Geophysics & Geomatics and Subsurface Multi-scale Imaging Lab (SMIL), State Key Laboratory of Geological Processes and Mineral Resources, China University of Geosciences, Wuhan 430074, China;

*E-mail: stzhao@cug.edu.cn

1. Introduction

Calcium carbonate is the primary compound of carbon reservoirs in the Earth's oceanic and continental crust. Biomineralization in the oceans is responsible for accumulation of hundred meters thick sequences of nannofossil oozes and chalks almost entirely composed of pure calcite (e.g., DSDP site 501 and 504 in the East Pacific, and site 212 in the Indian Ocean; Cann et al., 1983, and von der Borch et al., 1974). In the underlying igneous suites, hydrothermal fluids percolate to a depth of several kilometers, triggering the widespread precipitation of calcite and aragonite in vugs and veins (Bonatti et al. 1980; Alt and Teagle, 1999). Again, calcite cements serpentinized ultramafics in ophicarbonate breccias, which are produced in the highly tectonized oceanic litosphere, at slow spreading ridges, and at transform faults in fast spreading oceans. At continental margins, carbonate platforms are almost entirely built by organism fixing calcium carbonate.

Subduction and mantle convection are responsible for high-pressure and high-temperature reprocessing of Ca-carbonates in a diversity of thermo-mechanical scenarios, accounting for CO_2 sink in the frame of the global, long-term carbon cycle. Aragonite has been regarded since long time

as a marker of relatively low temperature - high pressure metamorphism, and it has been widely used in reference geobarometers for so-called ultra-high pressure metamorphic rocks (Hermann et al., 2016). Nonetheless, as Ca-carbonates are stable over a very wide range of temperatures (Suito et al., 2001; Li et al., 2017; Müller et al, 2017; Shatskiy et al. 2018), up to the average mantle adiabat beneath ridges and ocean islands (Fig. 1), a large range of carbonated eclogites and pyroxenites may contain aragonite at mantle conditions, as revealed by several experimental studies (Hammouda, 2003; Kiseeva et al., 2013; Grassi and Schmidt, 2011; Brey et al., 2015). Evidence of $CaCO_3$-bearing eclogitic assemblages have been also provided by the occurrence of inclusions of carbonates in the diamonds from Juina (Brazil), possibly originated from the lower part of the transition zone (Brenker et al., 2007), and of aragonite as inclusions in olivine phenocrysts from leucitite lava flows at Calatrava, Spain (Humphreys et al., 2010).

The geochemistry of carbonatites (Woolley and Kjarsgaard, 2008) and kimberlites (Becker and Le Roex, 2006) points to the importance of components CaO and CO_2 for describing their diversity and magmatic evolution. Carbonatites are thought to be among the major metasomatic agents in the sublithospheric mantle due to their low density, low viscosity and high reactivity (Green and Wallace, 1988). Whether calcite or aragonite occur on the liquidus surface it may affect the fractionation of trace elements as aragonite was experimentally found to preferentially partition Sr with respect to calcite (Carlson, 1980), and intermediate REE with respect to Fe-Mg carbonate (Brey et al., 2015).

Thermodynamic properties of $CaCO_3$ polymorphs, and of liquid $CaCO_3$, are barely known (Salje and Viswanathan, 1976; Redfern et al., 1989; Antao et al., 2009; Liu and Lange, 2003; O'Leary et al., 2015; Vuilleumier et al., 2014). Moreover, the volume equation of state of calcite V is substantially unknown at high temperature. Notably, the phase transition at high temperature from $CaCO_3$-polymorph calcite V to aragonite shows large discrepancies among the existing results (Fig. 1), and the behaviour of calcite V has been previously modelled extrapolating low-temperature

experimental data. Thermodynamic properties for a $CaCO_3$ component in liquid (hereafter $CaCO_3L$) is crucial for developing multi-component solution models suitable for predicting melting relations in carbonated mantle rocks, profiting of properties already available for $FeCO_3L$ (Kang et al., 2015) and $MgCO_3L$ (Kang et al., 2016).

Here we present an experimental study for the system $CaCO_3$ conducted with a multi-anvil apparatus at 3-6 GPa and 1300-1750 °C. In order to constrain the high temperature volume equation of state of calcite and aragonite, we additionally present in-situ X-ray diffraction experiments on calcite up to 1000 °C. Thermodynamic properties of aragonite, calcite V, and liquid $CaCO_3$ are derived by least-square fitting of experimental results and are used to calculate phase relations in carbonated eclogite composition where saturation in calcium carbonate is predicted over a wide range of pressures and temperatures, up to the *solidus*.

2. Experimental background on the system $CaCO_3$

Calcium carbonate ($CaCO_3$) is found in nature in three different structural forms: calcite (R-3c), aragonite (Pmcn), and vaterite (P63/mmc), although the stability field of vaterite is not well known (Maruyama et al., 2017). Aragonite generally represents the high-pressure and relatively low-temperature stable structure of $CaCO_3$, but it is commonly found as a metastable phase within the stability field of calcite, even at ambient conditions, due to its growth kinetics. At higher pressure, aragonite will transform to a post-aragonite phase at about 40 GPa (Merlini et al., 2016; Ono et al., 2007; Palaich et al., 2016).

Calcite has been reported with six different modification structures (calcite I, II, III, IV, V, and VI) over a wide range of pressure and temperature (Bagdassarov and Slutskii, 2003; Litasov et al., 2017; Mirwald, 1976; Redfern et al., 1989; Merlini et al., 2012). At room temperature, calcite I transforms into calcite II (monoclinic structure, P21/c) at 1.7 GPa and then to calcite III (C2) at 2.0 GPa (Smyth and Ahrens, 1997), which appears to persist to more than 6 GPa at very low-T

conditions (Suito et al., 2001). Calcite V, commonly regarded as disordered calcite, has been found at temperature higher than approximately 966 °C (Bagdassarov and Slutskii, 2003; Mirwald, 1976; Ishizawa et al., 2013), while calcite IV can be considered as an intermediate phase between calcite I to V related to disordering of the CO_3^{-2} groups (Ishizawa et al., 2013), above 700 °C. Transformation from phase IV into V is marked by the change of the space group from $R\bar{3}c$ to $R\bar{3}m$, with the c-length being halved. In Phase V, the oxygen atoms exist with equal probability along the undulated circular orbital around the central carbon.

The polymorphic transformation from trigonal calcite to orthorhombic aragonite is the most visible phase transition in the system $CaCO_3$. Nonetheless, previous studies aimed at defining the calcite-aragonite boundary yielded contradictory results, especially over the range of temperatures where calcite V is the stable low pressure phase (Fig. 1).

Experiments by Irving and Wyllie (1975) up to 3.5 GPa covered a temperature range from 800 °C to 1100 °C, and represent the solely synthesis reversals available where mixtures of both calcite and aragonite were used as starting materials. Their experimental data agree fairly well with the phase boundary calculated by Redfern et al. (1989) based on calorimetric measurements, and extrapolation of the calcite-aragonite transition curve to higher temperatures intersects $CaCO_3$-melting curve at an invariant point approximately located at 5.5 GPa and ~ 1650 °C (Irving and Wyllie, 1975). However, these results appear to be in poor agreement with DTA investigations on pure calcite by Mirwald (1976), and even contrast with in situ X-ray diffraction studies by Litasov et al. (2017), and Suito et al. (2001), where a disordered calcite was observed up to 6 GPa and 1230 °C that remains stable until melting (Fig. 1); the boundary aragonite-calcite suggested by Litasov et al. (2017) progressively increases its dP/dT slope until it becomes pressure insensitive above ~ 10 GPa at ~ 1300 °C. In-situ experiments are in substantial contrast with experimental results by Buob (2003), where $CaCO_3$ was found to maintain the aragonite structure up to 6 GPa and temperatures

between 1300-1500 °C, and by Shatskiy et al. (2014), where melting of aragonite was detected between 1600-1700 °C at 6 GPa.

The melting curve for $CaCO_3$ was recently investigated by Li et al. (2017) in the pressure range 3-21 GPa, based on *in situ* conductivity experiments; temperature of melting was detected on the basis of a steep and large rise in the ionic current through the sample during each heating cycle. Pre-melting peaks in the ionic current were attributed to phase transition from aragonite to calcite V, but results from marker experiments and Raman measurements of recovered samples exhibit aragonite in the P-T region where calcite V was supposed to be stable (Fig. 3b in Li et al., 2017). Melting of aragonite was bracketed down to 8 GPa by a falling Pt-sphere technique. Shatskiy et al. (2018) revisited the $CaCO_3$-$MgCO_3$ phase diagram and describe aragonite in equilibrium with melt at 6 GPa, in contrast with previous evidence (i.e. Litasov et al., 2017). A more recent paper, focussing on ultra-high pressure phase diagram of $CaCO_3$ (Bayarjgal et al., 2018) report in-situ experimental data indicating stability of aragonite at 11 GPa at temperatures higher than the stability line proposed by Litasov et al. (2017), indicating that further experimental work is mandatory to unravel the phase diagram reconstruction even at pressures beyond the range discussed here.

Currently available thermodynamic databases of petrological interest (Holland and Powell, 1998; update 2002; 2011) predict phase transformation of calcite to aragonite close to the experimental results of Mirwald (1976) at temperatures lower than ~ 1200 °C. It is worth noting that the 2002 update of the database by Holland and Powell (1998) includes a Landau model for aragonite, lately removed in Holland and Powell (2011), as aragonite does not exhibit disordering of CO_3 groups.

Synthesis, ex-situ, experiments, mostly cover the low-temperature, low-pressure range, whereas *in-situ* investigations mostly focus on the high-temperature, and high-pressure region of the phase diagram. Whether discrepancies should be partly ascribed to inter-laboratory pressure

124 calibration used is currently unclear; nonetheless, uncertainty on the location of the equilibrium
125 boundary close to the *solidus* is such that further data are mandatory to unravel appropriate
126 parameters for predicting the fate of carbonated eclogites at mantle pressure.

127 **3. Experimental and analytical techniques**

128 The experimental study was conducted in a 1000-ton Walker-type multi-anvil *apparatus* at the
129 Università degli Studi di Milano from 1300 °C to 1750 °C and 3 to 6 GPa. Experiments were all
130 performed in a multi-anvil apparatus, in order to provide the internal consistency of the data, after
131 recalibration of the pressure medium assembly (see Supplementary data A). In order to attain
132 textural equilibrium at run conditions, experiments at 1300-1500 °C were performed with a run
133 duration in the order of one day, whereas experiments at 1650-1750 °C lasted 1-2 hours. The
134 starting material was made of reagent-grade pure $CaCO_3$ powder (purity larger than 99.95%)
135 purchased from BDH Chemical Ltd, and synthetic aragonite.

136 The powders were permanently stored in a vacuum oven at 110 °C to prevent hydration, which
137 is known to cause a strong depression of $CaCO_3$ *solidus* temperature (Wyllie and Boettcher, 1969;
138 Müller et al 2017). Bracketing experiments were performed using starting materials containing both
139 reactants and products expected, in order to localize accurately the univariant equilibrium in the P-T
140 space (Pattison, 1994).

141 A 25/17 assembly was adopted to minimize thermal gradient in the run charge, using Cr_2O_3
142 doped MgO-octahedra, and preformed pyrophillite gaskets. The assembly includes ZrO_2 sleeve,
143 cylindrical graphite furnace, internal MgO spacers, and molybdenum end spacers ensuring electrical
144 contact. Temperature was controlled by Eurotherm controllers within ± 2°C, and monitored by S-
145 type ($Pt_{100}/Pt_{90}Rh_{10}$) axial thermocouples. Typical thermal gradient within the assembly is ± 20 °C
146 across the capsule. Starting material was loaded into a platinum capsule, and then stacked in the
147 central part of the furnace to minimize the uncertainty due to the thermal gradient across the sample

chamber. In order to reduce the influx of hydrogen during the experiments, as expected by the Soret effect, and then ensure a nearly-anhydrous run conditions, the capsule was packed with Fe_2O_3 powder before being embedded in a MgO sleeve (Liu and O'Neill, 2004).

At the end of the experiments, assembly was gradually decompressed overnight after quenching by shutting off the heating power. The averaged quench rate in the interval 500-1500 °C is around 400°C/sec, decreasing exponentially at lower temperatures. Recovered samples were longitudinally embedded in epoxy resins, ground and polished with diamond paste in order to expose a level of the product of synthesis, and finally carbon coated for Scanning Electron Microscope (SEM) analysis. Textural analysis of the phase assemblages was carried out by back-scattered (BSE), and secondary electrons imaging using a JEOL JXA8200 electron microprobe. Run products were also characterized by X-ray diffraction using Oxford X'calibur diffractometer (Mo X-ray source) available at the Department of Earth Sciences, University of Milan, to identify the mineral phases.

High temperature diffraction on $CaCO_3$ powder was performed at MCX beamline at Elettra synchrotron facility, using the high temperature furnace available and the standard experimental setup (Riello et al. 2013; Merlini et al., 2016). In-situ diffraction were collected in the temperature interval 25-1000°C, with sample contained in a quartz capillary connected to a CO_2 gas line at 1.5 bar to prevent decarbonation during the experiment (see the supplementary data B for details).

4. Results

A total of 11 successful synthesis experiments have been performed. Run conditions, duration of the experiments, and run products are reported in Table 1. Evidence for textural equilibration at subsolidus conditions comes from the development of polygonal grain boundaries and triple junctions between solid phases. Because $CaCO_3$ liquid phase does not quench to a glass, due to its low viscosity, melting in the system was inferred by the crystal morphologies that are

representatives of a textural disequilibrium, such as fibrous, elongated, or feather-like textures (Fig. 2) (Donaldson, 1976; Paterson, 1958).

The identification of $CaCO_3$ structural polymorph was based on X-ray powder diffraction (see supplementary data B). Since phase transformations from calcite I to IV, and V are unquenchable, the ex-situ characterization of high pressure experiments provide evidence for calcite I symmetry at ambient conditions for run products at 3.3 and 3.8 GPa, 1300 °C, and 3.8 GPa 1500 °C (Fig. 3). In-situ high-temperature experiments at ambient pressure show the peculiar thermal behaviour of calcite. A negative expansion of the a axis characterizes the structural evolution below approximately 600 °C. At this temperature the calcite to $CaCO_3$-IV transition is traditionally located. Whether $CaCO_3$-IV is a different polymorph of calcite or it represent a transitional behaviour of calcite is matter of debate. It is noticeable that the refinement of oxygen occupancy (see figure B4, supplementary data B) using a two carbonate group model, decrease starting at 600 °C and reach the 0.5 value of the fully disordered phase ($CaCO_3$-V) around 1000 °C.

Aragonite was detected at 4.2 GPa and 1300 °C, and remains stable up to 1650 °C at 4.7 GPa (Table 1, Fig. 3). It is extremely unlikely that aragonite occurrence in reversal experiments performed in this work represents the result of the conversion of a "disordered calcite" to aragonite on quenching. Reaction kinetics was found to be in the order of tens of hours at temperatures of 700 °C to achieve a complete transformation (Lin and Huang, 2004). This reconstructive transformation is therefore expected to be slow enough to be quenchable as drop in temperature from near solidus conditions to 700 °C occurs in a few seconds in multianvil apparatus.

Experimental brackets from this study, combined with data from previous works, were then used to constrain phase transition boundary from calcite V to aragonite, as well as $CaCO_3$ melting curve.

5. Thermodynamic modelling of Calcite V and $CaCO_3$L properties

196 **5.1 Locating the phase boundaries**

197 The transition boundary was thereby obtained by fitting the experimental brackets from this
198 study with the results from the ex-situ experimental results by Irving and Wyllie (1975), Buob
199 (2003) and Shatskiy et al (2014), an experimental dataset that does not support a positive change in
200 slope with increasing temperature as suggested by heating cycle experiments by Suito et al., (2001),
201 and by Litasov et al (2017)).

202 The calcite V-aragonite transition boundary can be expressed by the following first-order
203 equation:

204 $$T_{ccv-arag} = 320.17 \times P + 397.6 \qquad (1)$$

205 (P in GPa; T in K). This equation was then used, along with available thermodynamic data on
206 aragonite, to derive the thermodynamic properties of calcite V.

207 The melting curve for $CaCO_3$ was experimentally bracketed from 3-6 GPa. Melting of the
208 system was determined based on textural criterion through secondary electron imaging. Neither Ca-
209 oxides nor graphite nor gas bubbles were detected; run products were then interpreted in terms of
210 congruent melting:

211 $$CaCO_3 = liquid$$

212 since the quenched material consisted entirely of calcite. It is worth mentioning that incongruent
213 melting of $CaCO_3$ is expected to occur at low pressure (Wyllie and Boettcher, 1969).

214 $CaCO_3$-melting curve was determined by quadratic least square regression of experimental
215 brackets from this study combined with previously published data, and finally expressed by the
216 following quadratic polynomial between 0 and 4.5 GPa:

217 $$T_m = 1578.9 + 139.65 \times P - 11.646 \times P^2 \qquad (2)$$

218 , where P is in GPa and T in K. Equation 2 was successively used for modelling the thermodynamic
219 properties for $CaCO_3$-liquid.

220 **5.2 Retrieving thermodynamic data for calcite V and liquid $CaCO_3$**

221 Thermodynamic data on the pure substances $CaCO_3$, $MgCO_3$, and $FeCO_3$ constitute the basis for
222 modelling a ternary carbonate melt solution model, which is crucial for predicting natural
223 phenomena involving carbonates stability, carbonatite segregation, and metasomatic processes in
224 the mantle. However, while some properties have been already derived for iron (Kang et al., 2015)
225 and magnesium (Kang et al., 2016) carbonates, a model for high-temperature calcite consistent with
226 liquid calcium carbonate is still lacking. It is beyond the goal of this work to assess a model offering
227 a complete description of order-disorder phenomena accounting for the complexities of the
228 transformation from calcite I to calcite IV, and ultimately to calcite V (Ishizawa et al., 2013). Our
229 model is intended to reproduce properties and phase relationships at mantle temperatures and
230 pressures where either aragonite or calcite V is expected to be the stable phase.

231 Here we derive the standard molar Gibbs free energies G_0 (J), entropies S_0 (J/K), and selected
232 volumetric properties along with a revision of heat capacities at high temperature, by fitting the
233 energy residue at conditions of the calcite V-aragonite transition boundary (Eq. 1), where G_{ccv} =
234 G_{arag}, and along the $CaCO_3$ melting curve (Eq. 2), where $G_{ccv} = G_{CaCO3L}$.

235 Provided the large uncertainties at high temperature and the lack of data for ccV, the
236 temperature dependence of thermal expansivity (α_T), and of bulk modulus (K_T), are defined by the
237 approximations of Holland and Powell (2011) as:

238 $$\alpha_T = \alpha_0 \times \left(1 - \frac{10}{\sqrt{T}}\right) \quad (3)$$

239 $$K_T = K_0 \times [1 - 1.5 \times 10^{-4} \times (T - 298.15)] \quad (4)$$

240 Volume at reference pressure $V(T, P_r)$ is

$$V(T,P_r) = V_0 \times [1 + \int_{T-T_r}^{T} \alpha(T,P_r)dT] \quad (5)$$

, while volumes at elevated pressures are computed by the Murnaghan equation of state:

$$V(T,P) = V(T,P_r) \times \left[1 - K' \times \frac{P}{(K' \times P + K(T,P_r))}\right]^{\frac{1}{K'}} \quad (6)$$

The isobaric heat capacity function $C_p(T)$ adopted is from Holland and Powell (1998):

$$C_P = a + b \times T + \frac{c}{T^2} + \frac{d}{\sqrt{T}} \quad (7)$$

Coefficients for heat capacity functions for aragonite and calcite V were modified to converge to the Dulong-Petit limit at high temperature (> 2000 K) as:

$$C_P = 3 \times R \times n + \alpha_T^2 \times V_T \times K_T \times T \quad (8)$$

where R is the gas constant and n the number of atoms in the substance of interest. At low temperatures (< 800 K), the C_p functions converge the heat capacities after Holland and Powell (2011).

The heat capacity function for liquid $CaCO_3$ has the same form of that used for solids, as discussed in detail in Kang et al. (2015).

Gibbs free energies of crystalline calcite V, and of $CaCO_3$L, at the P-T conditions of the calcite V-aragonite transition, given by Eq. 1, and the $CaCO_3$ melting reaction, given by Eq. 2, respectively, were calculated from:

$$G(P,T) = G(P_r,T_r) - \int_{P_r,T_r}^{P_r,T} S(P_r,T)dT + \int_{P_r,T_r}^{P,T} V(P,T)dP$$

$$= G(P_r,T_r) + \int_{P_r,T_r}^{P_r,T} Cp(P_r,T)dT - T * \int_{P_r,T_r}^{P_r,T} [\frac{Cp(P_r,T)}{T}]dT + \int_{P_r,T_r}^{P,T} V(P,T)dP \quad (9)$$

The thermodynamic analysis was performed by adopting S_0 = 87.99 J/K of aragonite from Staveley and Linford (1969), later reported in Robie and Hemingway (1995), and G_0 of aragonite

averaging data from Robie and Hemingway (1995), and Königsberber et al. (1999). V_0, α_0, K_0 and K' of aragonite from the data presented in Palaich et al. (2016) re-fitted with eq. (6). The volume equation of state of calcite V is substantially unknown at high temperature; we therefore collected in-situ X-ray diffraction on $CaCO_3$ in order to determine thermal expansivity. Thermal expansion of calcite results increases from 4.1E-5 m/°C determined in the 25-500 °C interval (Merlini et al., 2016) up to 1.34E-4 m/°C in the highest temperature range investigated here. As a consequence G_0 and S_0 of calcite V were fitted adopting V_0 at 3.60 J/bar, and fitting α_0 constrained at values higher than 1.0E-4 m/°C. Bulk modulus of calcite and its derivative were derived from Merlini et al (2016). Thermodynamic properties for liquid $CaCO_3$ were derived assuming a fixed bulk modulus derivative (K' = 4.0) (Kang et al., 2016). The results of the non-linear least-square fit are presented in Table 2.

The dependence of density on temperature and pressure for liquid $CaCO_3$ was calculated by Perple_X thermodynamic software (Connolly, 2005), at conditions of 1773 and 2073 K. Results are compared with those provided by molecular dynamics (MD) calculations implemented by empirical pair potential force field, and those evaluated by first-principle molecular dynamics (FPMD) proposed by Vuilleumier et al. (2014) fitted with Birch-Murnaghan equation of state and those obtained with the radial distribution functions by Hudspeth et al. (2018). The EoS retrieved from our study results in a compressibility for the $CaCO_3$-liquid intermediate between those proposed by Vuilleumier et al. (2014) and Hudspeth et al. (2018) (Fig. 5). It is worth pointing out that our thermodynamic data retrieved for liquid $CaCO_3$ entirely derive from the melting curve of calcite V, with no additional constrain; as a consequence the agreement of the pressure dependence for density as calculated here and as obtained by independent methods is quite remarkable.

6. Discussion

6.1 Phase relationships in the system $CaCO_3$

285 Phase relationships have been calculated in the system $CaCO_3$ at pressures to 10 GPa using the
286 thermodynamic parameters for $CaCO_3$ provided from this study, and, for comparison, from Holland
287 and Powell (2011), and 2002 update of database in Holland and Powell (1998), hereafter
288 abbreviated as HP11 and HP02, respectively. The calculated results are compared with previously
289 published experimental data by Irving and Wyllie (1975) (IW75), Suito et al. (2001) (S01), Buob
290 (2003) (B03), Shatskiy et al. (2014) (S14) and Li et al. (2017) (Li17) (Fig.3).

291 As previously stated, it is beyond the goal of this work to offer a model reproducing the
292 transformations calcite I-IV-V. Thermodynamic data for calcite V were not optimized at low
293 temperature, resulting in a stability field for disordered calcite extending down to temperature of
294 approximately 610 °C; it is worth remembering that disordering to calcite IV in calcite was
295 observed from approximately 700 °C at nearly room pressure (Ishizawa et al., 2013)

296 At relatively low-pressures and low-temperature, the calcite V-aragonite boundary modelled
297 by employing our dataset does not differ significantly with that predicted by HP11, and HP02,
298 database (dashed, and dotted lines in Fig. 3, respectively). However, with increasing temperature,
299 larger deviations occur among the calculated results: HP11, and HP02 databases predict an
300 increasingly steepening slope for the calcite V - aragonite boundary, such that aragonite is not
301 expected to participate to melting in the uppermost mantle. On the contrary, the boundary
302 determined by our model maintains an almost constant dP/dT, then encountering the invariant point
303 calcite V - aragonite - liquid at about 5 GPa and 1650 °C, which matches fairly well with the
304 invariant point experimentally extrapolated by Irving and Wyllie (1975), and the shape of the
305 solidus, as determined by Li et al. (2017). Additionally, the stability field that we report for
306 aragonite covers the P-T conditions where aragonite was observed as the stable polymorph by Buob
307 (2003), and by Shatskiy et al. (2014).

At pressure above 8 GPa, the melting curve exhibits a moderately negative slope, then suggesting that the liquid becomes more compressible than the solid, as it was also expected by both *ab initio* simulations and *in-situ* conductivity experiments by Li et al. (2017).

6.2 Modelling experimentally constrained carbonated-eclogite

To further test the reliability of our thermodynamic model, pseudosections have been performed on experimentally constrained complex chemical systems (Table 3), such as *bulk* compositions OTBC (carbonated eclogite with the altered basalt composition (OTB) + 10.1 wt% calcite + 0.12 wt% water bulk composition, Hammouda, 2003), SLEC1 (carbonated eclogite, Dasgupta et al., 2004), GA1cc (eclogite composition of GA1, representing altered oceanic MOR basalt, +10% $CaCO_3$, Kiseeva et al., 2013) and EC1 (carbonate-bearing eclogite assemblages, Yaxley and Brey, 2004), that are generally referred to as mantle heterogeneites derived from deeply recycled, subducted oceanic crust (Fig. 6 and 7). For comparison, phase relationships have been modelled by using the thermodynamic properties for $CaCO_3$ from both this study, and HP11 database.

The bulk composition OTBC (Hammouda, 2003) represents a partially hydrated carbonated eclogite (0.12 wt.% H_2O in the starting material). Its re-equilibration at mantle conditions, promoted by the deep recycling of oceanic material, may account for the extraction of carbonate-rich liquids. We performed pseudosections with the Perple_X thermodynamic calculators (Connolly, 2005), on a K-free OTBC from 1-10 GPa and 900-1300 °C by implementing the thermodynamic dataset for $CaCO_3$ retrieved from this study (Fig. 6a), and then compared the results with those obtained by employing the parameters for $CaCO_3$ provided by the HP11 database (Fig. 6b). Solution models for clinopyroxene, spinel, plagioclase, and garnet used here are from Jennings and Holland (2015), for binary H_2O-CO_2 fluid from Connolly and Trommsdorff (1991), and for ternary Ca–Fe–Mg carbonates from Franzolin et al. (2011). The latter model is able to predict immiscibilities in carbonate solid solutions. The pseudosection presents a clinopyroxene - garnet - coesite assemblage

stable over a large range of P-T conditions (Fig. 6), while plagioclase only occurs at pressures lower than ~ 2.5 GPa. From 1 to ~ 4 GPa, the eclogitic assemblages coexist with a magnesian-calcite solid solution (X_{Ca} > 0.8), whereas at higher pressures the stable carbonate phases are aragonite, and aragonite + magnesite with increasing pressure. Aragonite stability field covers a wide P-T range, extending down to 4 GPa at 1300 °C; the abundance of aragonite calculated for this bulk composition reaches approx. 11 wt.% in the region 4 - 5 GPa at 1000 °C, and 7 - 10 GPa at 1300 °C.

The calculation performed with our dataset was found to well reproduce the experimental results especially in the high-pressure region, as the association aragonite + magnesite was detected at near-*solidus* conditions from 7 to 10 GPa (Hammouda, 2003). The abundance that have been obtained for aragonite agrees fairly well with its ubiquitous presence in the experiments at pressures higher than 6 GPa; above this pressure, aragonite was found to persist largely above the experimentally determined solidus (Fig. 6a), up to 1200 °C where it coexists with a carbonatitic melt (Hammouda, 2003). Although a model for carbonatitic liquids cannot be constructed here because of the large non-ideality of $CaCO_3$ - $MgCO_3$ - $FeCO_3$ plane, we expect that the calculated abundance of aragonite correlates with likelihood of its occurrence at supersolidus conditions, notably when the liquid is silicate. The development of a thermodynamic model for describing the liquidus surface of ternary carbonatitic liquids will be discussed elsewhere.

The phase diagram calculated by employing the $CaCO_3$ parameters from HP11 (Fig. 6b) reveals major differences in a P-T region, between 1100-1300 °C and 4-6 GPa, which is most relevant for magma generation and where transition from carbonate to silicate melt was inferred to occur (Hammouda, 2003). We speculate that aragonite is expected to be entirely consumed approaching the solidus according to HP11 database, whereas the adoption of our new thermodynamic dataset (Fig. 6b) show that aragonite might persist with the liquid, as observed at higher pressures. The implications of this will be discussed below.

358 The stability of aragonite within an eclogitic assemblages was also verified at conditions of the
359 mantle transition zone, by Kiseeva et al. (2013) on carbonated eclogite, GA1cc. Thermodynamic
360 modelling (not shown) define a dominant eclogitic association, given by clinopyroxene, garnet and
361 coesite/stishovite, coexisting with aragonite + magnesite.

362 In order to constrain the variability of aragonite occurrence within eclogitic systems where
363 $CaCO_3$-saturation was not experimentally observed, pseudosections were also performed, by
364 employing our new dataset, on *bulk* compositions SLEC1 (Dasgupta et al., 2004) and EC1 (Yaxley
365 an Brey, 2004). The thermodynamic calculation performed on SLEC1 (K-free, Mn-free for sake of
366 simplicity) exhibits very small fractions of aragonite (<1 wt%), limited to pressures higher than 5
367 GPa (Fig. 7a); the computed results are in substantial accord with the experimental record, where
368 only calcian-dolomite solid solution, and magnesite at higher pressure, were found at near-*solidus*
369 conditions, whereas aragonite is not obvserved. Differently, the pseudosection calculation
370 performed on EC1 composition displays a large P-T range where aragonite forms, reaching modal
371 contents of up to 20 wt % at high pressure (Fig. 7b). However, aragonite was not observed by
372 Yaxley and Brey (2004), as the range of pressures and temperatures investigated (2.5-5.5 GPa and
373 ~1125-1310°C) were just below the stability field predicted by our calculations. The bulk
374 composition EC1 is most suitable to highlight the relevance of aragonite at upper mantle conditions.

375 **6.3 Aragonite stability in mantle heterogeneities**

376 The new set of thermodynamic parameters for $CaCO_3$ was found to describe properly phase
377 relationships in carbonated eclogites, which are regarded as potential sources for feeding
378 carbonatitic and silica undersaturated basaltic magmas observed within intra-plate environments
379 (Sobolev et al., 2005; Aulbach et al., 2017). The geochemical signature exhibited by these
380 magmatic suites are interpreted to derive from an eclogitic component, inherited by a deeply
381 subducted oceanic crust (Hofmann, 1997; Kogiso et al., 1997); therefore, the *bulk* composition of
382 such recycled material may span a wide compositional range in major elements (Hirschmann and

383 Stolper, 1996), notably due to the heterogeneous extent of the primeval ocean floor alteration, and
384 of the subsequent dehydration processes during subduction. Phase assemblages and melting
385 reactions within mantle heterogeneites are not univocal in the P-T space, but largely differ
386 depending on several compositional effects.

387 The initial *bulk* #Ca ratio, Ca/(Ca + Mg + Fe) was found to strongly determine the carbonated-
388 eclogite melting temperature and chemical features of liquid produced, due to the location of the
389 minimum of the liquidus surface on the binary $CaCO_3$-$MgCO_3$ (Irving and Wyllie 1975). The
390 composition of dolomite, and magnesian-calcite solid solution at near-*solidus* is buffered by the
391 partitioning of Ca-Mg with silicates, mainly garnet and clinopyroxene, which in turn depends on the
392 contents of Al_2O_3 and Na_2O in the bulk composition. These compositional parameters partly
393 account for the large discrepancies on the location of the carbonated-eclogite *solidus* curve, which
394 may differs by the order of ~ 200 °C between the experimental determination on SLEC1 (Dasgupta
395 et al., 2004), EC1 (Yaxley and Brey, 2004), and OTBC (Hammouda, 2003). The very high melting
396 temperature recorded on EC1 is likely to be related to the high #Ca values (#Ca = 0.435), along
397 with high CO_2 contents (15.38 wt.%), with respect to the SLEC1 composition (#Ca = 0.319, CO_2 =
398 5 wt.%), whereas the relatively low-T *solidus* determined on OTBC is probably due to the presence
399 of H_2O, which is known to strongly depress the melting temperature on #Ca-rich systems (Poli,
400 2015).

401 Aragonite is often referred to as a phase relevant at relatively low-T conditions, and commonly
402 associated to subduction zone processes. However, the relevance of aragonite in the generation and
403 evolution of igneous suites is testified by its occurrence in metasomatized pyroxenites from the
404 North Andean mantle (Ferri et al, 2017) and in alkaline lavas from Clatrava, Spain (Humphreys et
405 al., 2010). The stability of aragonite not simply correlates to the amount of CaO in the bulk
406 composition, but more closely relates to availability of alumina. The higher the Al_2O_3, the larger the
407 fraction of Mg and Fe fractionated in garnet, the higher the "residue" of CaO available to form a

408 calcium carbonate component (Fig. 8), if CO_2 is available. As a consequence, although the *bulk*
409 composition SLEC1 adopted by Dasgupta et al. (2004) to model the solidus of carbonated eclogites
410 is relatively enriched in CaO, the low alumina content drives the composition toward the
411 $(Mg,Fe)CO_3$ component, when compared to other experimentally investigated *bulk* compositions
412 (compare Figs. 6 and 7).

413 The role of aragonite on controlling the melting temperatures in eclogitic systems remains
414 unclear, but the relevance of the assemblage aragonite + magnesite-siderite solid solution at high-
415 pressure, at near-*solidus* conditions, was both thermodynamically predicted (in this study) and
416 experimentally testified in Hammouda (2003), and Kiseeva et al. (2013). It is worth remembering
417 that a carbonate, namely aragonite, and graphite or diamond are not mutually exclusive in complex
418 bulk composition. A field exists in the log fO_2 vs. P-T space where carbonates coexist with
419 elemental carbon, and the lower the temperature, the larger the log fO_2 interval (see Fig 3 in Poli et
420 al., 2009).

421

422 **7. Implications for the geochemical signature of anorogenic magmas**

423 The thermodynamic properties for aragonite, calcite V, and $CaCO_3L$, were derived here by a
424 least-square fitting analysis of the experimental data available. The boundary of phase transition
425 from calcite V to aragonite, and the melting curve of $CaCO_3$, were provided in a P-T region relevant
426 for investigating processes in the upper mantle. We revisited the aragonite stability field, which was
427 found to extend to lower pressures and, relatively, higher temperatures in comparison to what it has
428 been recently assessed on the basis of in-situ experiments and previous thermodynamic modelling.
429 *In-situ* XRD studies (Suito et al., 2001; Litasov et al., 2017) restricted aragonite stability, yielding
430 results conflicting with *synthesis* experiments where aragonite has been observed up to the melting
431 curve at pressures as low as 4.7 GPa.

The modelling of carbonated-eclogites shows that aragonite may occur as a major compound in a range of P-T conditions where melting reactions have been experimentally determined (Hammouda, 2003; Kiseeva et al., 2013). It is widely accepted since long time that the composition of carbonatitic and kimberlitic melts requires a metasomatized mantle source (Wyllie, 1980; Ringwood et al., 1992; Eggler, 1978). The extended stability of aragonite may drive significant fractionation of trace elements in such coexisting liquids because solid-melt trace elements partition coefficients for aragonite are drastically different from those determined for magnesite or silicates (Brey et al., 2015). Aragonite strongly sequesters REE, notably intermediate REE, and Sr, whereas HFS elements result highly incompatible, to a larger extent than magnesite (see Fig. 8 in Brey et al., 2015). Figure 9 highlights the peculiar geochemical signature of aragonite, with reference to the Primitive Mantle of Sun and McDonough (1989). Fractionation of aragonite from a segregated, mobile, volatile enriched liquid would therefore contribute to the definition of a typical anorogenic signature as observed for those silica undersaturated magmas, where a carbonatitic component is claimed, including kimberlites (Becker and Le Roex, 2006).

As H_2O strongly depresses the *solidus* temperature of carbonated lithologies enriched in Ca, the generation of hydrous carbonatitic liquids is potentially extended to subduction zone tectonic settings (Poli 2015, 2016). How aragonite participates to melting reactions at such conditions is currently unknown, and trace element pattern fractionation might significantly differ from anorogenic settings, provided the expected dissimilarity in H_2O availability and thermal field.

Aragonite is expected to be a major player in the evolution of a mantle refertilized by deeply subducted altered oceanic crust, as it persists to hot mantle adiabats and provides a mean to fractionate trace elements at the onset of melting. Further investigations are mandatory for unravelling the complex interplay between carbonates and H_2O components in mantle heterogeneities, and how their relationships eventually govern the geochemical evolution of intra-plate magmatism.

Acknowledgments

The constructive reviews by Donato Belmonte and by an anonymous reviewer significantly improved the manuscript. We acknowledge Elettra synchrotron facility for provision of beamtime at the MCX beamline; Jasper Plaiser and Lara Gigli are acknowledged for helpful assistance as local contacts. This work has been supported by the NSF of China (Grant No. 41204060), and Scholarship support to S.Z. as Visiting Scholar from China Scholarship Council during her stay at Milan University is greatly appreciated. E.S. and S.P. acknowledge support from the Deep Carbon Observatory (DCO).

References

Alt, J. C. and Teagle, D. A. H., 1999. The uptake of carbon during alteration of ocean crust. Geochimica et Cosmochimica Acta 63, 1527-1535.

Antao, S. M., Hassan, I., Mulder, W. H., Lee, P. L., Toby, B. H., 2009. In situ study of the R3c → R3m orientational disorder in calcite. Physics and Chemistry of Minerals 36, 159-169.

Aulbach, S., Massuyeau, M., Gaillard, F., 2017. Origins of cratonic mantle discontinuities: A review from petrology, geochemistry and thermodynamic models. Lithos 268-271, 364-382.

Bagdassarov, N. S. and Slutskii, A. B., 2003. Phase transformations in calcite from electrical impedance measurements. Phase Transition 76, 1015-1028.

Bayarjargal, L., Fruhner, C. J., Schrodt, N., Winkler B., 2018. $CaCO_3$ phase diagram studied with Raman spectroscopy at pressures up to 50 GPa and high temperatures and DFT modelling. Physics of the Earth and Planetary Interiors 281, 31-45.

Becker, M., and Le Roex, A. P., 2006. Geochemistry of South African on - and off-craton, Group I and Group II kimberlites: petrogenesis and source region evolution. Journal of Petrology 47, 673-703.

Bonatti, E., Lawrence, J. R., Hamlyn, P. R., Breger, D, 1980. Aragonite from deep sea ultramafic. Geochimica et Cosmochimica Acta 44, 8, 1207-1214.

Brenker, F. E., Vollmer, C., Vincze, L., Vekemans, B., Szymanski, A., Janssens, K., Szaloki, I., Nasdala, L., Joswig, W., Kaminsky, F., 2007. Carbonates from the lower part of the transition zone or even the lower mantle. Earth and Planetary Science Letters 260, 1–9.

Brey, G. P., Girnis, A.V., Bulatov, V. K., Höfer, H. E., Gerdes, A., Woodland, A. B., 2015. Reduced sediment melting at 7.5-12 GPa: phase relations, geochemical signals and diamond nucleation. Contributions to Mineralogy and Petrology 170, 18.

490 Buob, A., 2003. The system $CaCO_3$-$MgCO_3$: experiments and thermodynamic modelling of the
491 trigonal and orthorhombic solid solutions at high pressure and temperature. 109 p. Ph.D. thesis,
492 Swiss Federal Institute of Technology, Zurich.

493 Cann, J. R., Langseth, M. G., Honnorez, J., Von Herzen, R. P., White, S. M., and the Shipboard
494 Scientific Party (1983) 2. Sites 501 and 504: Sediments and Ocean Crust in an Area of High Heat
495 Flow on the Southern Flank of the Costa Rica Rift. Initial Reports DSDP 69, 31-173.

496 Carlson, W., 1980. The calcite-aragonite equilibrium: effects of Sr substitution and anion
497 orientational disorder. American Mineralogist 65, 1252-1262.

498 Connolly, J. A. D., 2005. Computation of phase equilibria by linear programming: a tool for
499 geodynamic modelling and its application to subduction zone decarbonation. Earth and Planetary
500 Science Letters 236, 524-541.

501 Connolly, J. A. D., and Trommsdorff, V., 1991. Petrogenetic grids for metacarbonate rocks:
502 pressure-temperature phase-diagram projection for mixed-volatile systems. Contributions to
503 Mineralogy and Petrology 108, 93-105.

504 Dasgupta, R., and Hirschmann, M.M., 2010. The deep carbon cycle and melting in Earth's interior.
505 Earth and Planetary Science Letters 298, 1-13.

506 Dasgupta, R., Hirschmann, M. M., Withers, A. C., 2004. Deep Global cycling of carbon constrained
507 by the solidus of anhydrous, carbonated eclogite under upper mantle conditions. Earth and
508 Planetary Science Letters 227, 73-85.

509 Donaldson, C. H., 1976. An experimental investigation of olivine morphology. Contribution to
510 Mineralogy and Petrology 57, 187-213.

511 Eggler, D. H. 1978. Stability of dolomite in a hydrous mantle, with implications for the mantle
512 solidus. Geology 6, 397-400.

513 Ferri, F., Poli, S., Rodríguez-Vargas, A., 2017. Andean Volcanoes Record Carbonatite Mantle
514 Metasomatism and CO2 Degassing at Subduction Zones. Goldschmidt2017 Abstract 05b, 2157.

515 Franzolin, E., Schmidt, M. W., Poli, S., 2011. Ternary Ca-Fe-Mg carbonates: subsolidus phase
516 relations at 3.5 GPa and a thermodynamic solid solution model including order/disorder.
517 Contributions to Mineralogy and Petrology 161, 213-227.

518 Grassi, D., and Schmidt, M. W., 2011. The melting of carbonated pelites from 70 to 700 km depth.
519 Journal of Petrology 52, 4, 765-789.

520 Green, D. H., and Wallace, M. E., 1988. Mantle metasomatism by ephemeral carbonatite melts.
521 Nature 336, 459-462.

522 Hammouda, T., 2003. High-pressure melting of carbonated eclogite and experimental constraints on
523 carbon recycling and storage in the mantle. Earth and Planetary Science Letters 214, 357-368.

524 Hermann, J., Troitzsch, U., Scott, D., 2016. Experimental subsolidus phase relations in the system
525 $CaCO_3$-$CaMg(CO_3)_2$ up to 6.5 GPa and implications for subducted marbles. Contributions to
526 Mineralogy and Petrology 171, 84.

527 Hirschmann, M. M., and Stolper, E. M., 1996. A possible role of garnet pyroxenite in the origin of
528 the "garnet signature" in the MORB. Contributions to Mineralogy and Petrology 124, 185-208.

529 Hofmann, A. W. 1997. Mantle geochemistry; the message from oceanic volcanism. Nature 385,
530 219-229.

531 Holland, T. J. B., and Powell, R., 1998. An internally consistent thermodynamic dataset for phases
532 of petrological interest. Journal of Metamorphic Geology16, 309-343.

533 Holland, T. J. B., and Powell, R., 2011. An improved and extended internally consistent
534 thermodynamic dataset for phases of petrological interest, involving a new equation of state for
535 solids. Journal of Metamorphic Geology 29, 333-383.

536 Hudspeth, J., Sanloup, C., Kono, Y., 2018. Properties of molten $CaCO_3$ at high pressure.
537 Geochemical Perspectives Letters **7**, 17-21.

538 Humphreys, E. R., Bailey, K., Hawkesworth, C. J., Wall, F., Najorka, J., Rankin, A. H., 2010.
539 Aragonite in olivine from Calatrava, Spain – Evidence for mantle carbonatite melts from > 100 km
540 depth. Geology 38, 911-914.

541 Irving, A. J., and Wyllie, P. J., 1975. Subsolidus and melting relationships for calcite, magnesite
542 and the join $CaCO_3$-$MgCO_3$ to 36 kb. Geochimica et Cosmochimica Acta 39, 35-53.

543 Ishizawa, N., Setoguchi, H., Yanagisawa, K., 2013. Structural evolution of calcite at high
544 temperatures: phase V unveiled. Scientific Reports 3, 2832.

545 Jennings, E. S., and Holland, T. J. B., 2015. A simple thermodynamic model for melting of
546 peridotite in the system NCFMASOCr. Journal of Petrology 56, 869-892.

547 Kang N., Schmidt, M. W., Poli, S., Franzolin, E., Connolly, J. A. D., 2015. Melting of siderite to 20
548 GPa and thermodynamic properties of $FeCO_3$-melt. Chemical Geology 400, 34-43.

549 Kang, N., Schmidt, M. W., Poli, S., Connolly, J. A. D., Franzolin, E., 2016. Melting relations in the
550 system $FeCO_3$-$MgCO_3$ and thermodynamic modelling of Fe-Mg carbonate melts. Contributions to
551 Mineralogy and Petrology 171, 74.

552 Kelemen, P. B., Hanghøj, K., Greene, A. R., 2003. One view on the geochemistry of subduction-
553 related magmatic arcs, with an emphasis on primitive andesites and lower crust. Treatise on
554 Geochemistry 3, 593-659.

555 Kiseeva, E. S., Litasov, K. D., Yaxley, G. M., Ohtani, E., Kamenetsky, V. S., 2013. Melting and
556 phase relations of carbonated eclogite at 9-21 GPa and the petrogenesis of alkali-rich melts in the
557 deep mantle. Journal of Petrology 54, 8, 1555-1583.

Kogiso, T., Tatsumi, Y., Shimoda, G., Barsczus, H. G., 1997. High μ (HIMU) ocean island basalts in southern Polynesia: new evidence for whole mantle scale recycling of subducted oceanic crust. Journal of Geophysical Research 102, 8085-8103.

Königsberger, E., Königsberger, L. C., Gamsjäger, H., 1999. Low-temperature thermodynamic model for the system Na_2CO_3-$MgCO_3$-$CaCO_3$-H_2O. Geochimica et Cosmochimica Acta 63, 3105-3119.

Li, Z., Li, J., Lange, R., Liu, J., Militzer, B., 2017. Determination of calcium carbonate and sodium carbonate melting curves up to Earth's transition zone pressures with implications for the deep carbon cycle. Earth and Planetary Science Letters 457, 395-402.

Lin, S. J., and Huang, W. L., 2004. Polycrystalline calcite to aragonite transformation kinetics: experiments in synthetic systems. Contributions to Mineralogy and Petrology 147, 604-614.

Litasov, K. D., Shatskiy, A., Gavryushkin, P. N., Bekhtenova, A. E., Dorogokupets, P. I., Danilov, B. S., Higo, Y., Akilbekov, A. T., Inerbaev, T. M., 2017. P-V-T equation of state of $CaCO_3$ aragonite to 29 GPa and 1673 K: In situ X-ray diffraction study. Physics of the Earth and Planetary Interiors 265, 82-91.

Liu, Q., and Lange, R. A., 2003. New density measurements on carbonate liquids and the partial molar volume of the $CaCO_3$ component. Contributions to Mineralogy and Petrology 146, 370-381.

Liu, X., O'Neill, H. S. C., 2004. The effect of Cr_2O_3 on the partial melting of spinel lherzolite in the system CaO-MgO-Al_2O_3-SiO_2-Cr_2O_3 at 1.1 GPa. Journal of Petrology 45, 2261-2286.

Maruyama, K., Kagi, H., Komatsu, K., Yoshino, T., Nakano, S., 2017. Pressure-induced phase transitions of vaterite, a metastable phase of $CaCO_3$. Journal of Raman Spectroscopy 48, 1449-1453.

580 Merlini, M., Hanfland, M., Crichton, W. A., 2012. $CaCO_3$-III and $CaCO_3$-VI, high-pressure
581 polymorphs of calcite: Possible host structures for carbon in the Earth's mantle. Earth and Planetary
582 Science Letters 333-334, 265-271.

583 Merlini, M., Sapelli, F., Fumagalli, P., Gatta, G. D., Lotti, P., Tumiati, S., Abdellatief, M., Lausi,
584 A., Plaisier, J., Hanfland, M., Crichton, W., Chantel, J., Guignard, J., Meneghini, C., Pavese, A.,
585 Poli, S., 2016. High-temperature and high-pressure behaviour of carbonates in the ternary diagram
586 $CaCO_3$-$MgCO_3$-$FeCO_3$. American Mineralogist 101, 1423-1430.

587 Mirwald, P. W., 1976. A differential thermal analysis study of the high-temperature polymorphism
588 of calcite at high pressure. Contributions to Mineralogy and Petrology 59, 33-40.

589 Müller, I. A., Violay, M. E. S., Storck, J. C., Fernandez, A., van Dijk, J., Madonna, C., Bernasconi,
590 S. M., 2017. Clumped isotope fractionation during phosphoric acid digestion of carbonates at 70
591 degrees C. Chemical Geology 449, 1-14.

592 O'Leary, M. C., Lange, R. A., Ai, Y., 2015. The compressibility of $CaCO_3$-Li_2CO_3-Na_2CO_3-K_2CO_3
593 liquids: application to natrocarbonatite and CO_2-bearing nephelinite liquids from Oldoinyo Lengai.
594 Contributions to Mineralogy and Petrology 170, 3.

595 Ono, S., Kikegawa, T., Ohishi, Y., 2007. High-pressure transition of $CaCO_3$. American
596 Mineralogist 92, 1246-1249.

597 Palaich, S. E. M., Heffern, R. A., Hanfald, M., Lausi, A., Kavner, A., Manning, C. E., Merlini, M.,
598 2016. High-pressure compressibility and thermal expansion of aragonite. American Mineralogist
599 101, 1651-1658.

600 Paterson, M. S., 1958. The melting of Calcite in the presence of water and carbon dioxide.
601 American Mineralogist 43, 603-606.

602 Pattison, D. R. M., 1994. Are reversed Fe-Mg exchange and solid solution experiments really
603 reversed? American Mineralogist 79, 938-950.

604 Poli, S., Franzolin, E., Fumagalli, P., Crottini A., 2009. The transport of carbon and hydrogen in
605 subducted oceanic crust: An experimental study to 5 GPa. Earth and Planetary Science Letters 278,
606 350-360.

607 Poli, S., 2015. Carbon mobilized at shallow depths in subduction zones by carbonatitic liquids.
608 Nature Geoscience 8, 633-636.

609 Poli, S., 2016. Melting carbonated epidote eclogites: carbonatites from subducting slabs. Progress in
610 Earth and Planetary Science 3, 27.

611 Redfern, S. A. T., Salje, E., Navrotsky, A., 1989. High-temperature enthalpy at the orientational
612 order-disorder transition in calcite: implications for the calcite/aragonite phase equilibrium.
613 Contributions to Mineralogy and Petrology 101, 479-484.

614 Riello, P., Lausi, A., MacLeod, J., Plaisier, J. R., Zerauschek, G., Fornasiero, P., 2013. In situ
615 reaction furnace for real-time XRD studies. Journal of Synchrotron Radiation 20, 194-196.

616 Ringwood, A. E., Kesson, S. E., Hibberson, W., Ware, N., 1992. Origin Of Kimberlites And
617 Related Magmas. Earth and Planetary Science Letters 113, 521-538.

618 Robie, R. A., and Hemingway, B. S., 1995. Thermodynamic properties of minerals and related
619 substances at 298.15 K and 1 Bar (105 Pascals) pressure and at higher temperatures. U.S.
620 Geological Survey Bullettin 2131.

621 Salje, E., and Viswanathan, K., 1976. The phase diagram calcite-aragonite as derived from
622 crystallographic properties. Contributions to Mineralogy and Petrology 55, 55-67.

623 Shatskiy, A., Borzdov, Y. M., Litasov, K. D., Kupriyanov, I. N., Ohtani, E., Palyanov, Y. N., 2014.
624 Phase relations in the system $FeCO_3$-$CaCO_3$ at 6 GPa and 900-1700 °C and its relation to the
625 system $CaCO_3$-$FeCO_3$-$MgCO_3$. American Mineralogist 99, 773-785.

626 Shatskiy, A., Podborodnikov, I. V., Arefiev, A. V., Minin, D. A., Chanyshev, A. D., Litasov, K. D.,
627 2018. Revision of the $CaCO_3$-$MgCO_3$ phase diagram at 3 and 6 GPa. American Mineralogist 103,
628 441-452.

629 Smyth, J. R., and Ahrens, T. J., 1997. The crystal structure of calcite III. Geophysical Research
630 Letters 24, 1595-1598.

631 Sobolev, A. V., Hofmann, A. W., Sobolev, S. V., and Nikogosian, I. G., 2005. An olivine-free
632 mantle source of Hawaiian shield basalts. Nature 434, 590-7.

633 Staveley, L. A. K., and Linford, R. G., 1969. The heat capacity and entropy of calcite and aragonite,
634 and their interpretation. Journal of Chemical Thermodynamics 1, 1-11.

635 Suito, K., Namba, J., Horikawa, T., Taniguchi, Y., Sakurai, N., Kobayashi, M., Onodera, A.,
636 Shimomura, O., Kikegawa, T., 2001. Phase relations of CaCO3 at high pressure and high
637 temperature. American Mineralogist 86, 997-1002.

638 Sun, S. S., and McDonough, W. F., 1989. Chemical and isotopic systematics of oceanic basalts:
639 implications for mantle composition and processes. Geological Society, London, Special
640 Publications, 42, 313-345.

641 von der Borch, C.C., and the Shipboard Scientific Party (1974) Site 212. Initial Reports DSDP 22,
642 37-83.

643 Vuilleumier, R., Seitsonen, A., Sator, N., Guillot, B., 2014. Structure, equation of state and
644 transport properties of molten calcium carbonate ($CaCO_3$) by atomistic simulations. Geochimica et
645 Cosmochimica Acta 141, 547-566.

646 Woolley, A. R., and Kjarsgaard, B. A., 2008. Paragenetic types of carbonatite as indicated by the
647 diversity and relative abundances of associated silicate rocks: evidence from global database. The
648 Canadian Mineralogist 46, 741-752.

649 Wyllie, P. J., 1980. The origin of kimberlite. Journal of Geophysical Research 85, 6902–6910.

650 Wyllie, P. J., and Boettcher, A. L., 1969. Liquidus phase relationships in the system CaO-CO_2-H_2O
651 to 40 kilobars pressure with petrological applications. American Journal of Science 267-A , 489-
652 508.

653 Yaxley, G. M., and Brey, G. P., 2004. Phase relations of carbonate-bearing eclogite assemblages
654 from 2.5 to 5.5 GPa: implications for petrogenesis of carbonatites. Contributions to Mineralogy and
655 Petrology 146, 606-619.

656

657

658

659

660

661

662

663

664

665

666

667 **Figure captions**

668 **Figure 1**

669 Summary of the phase relations in the system $CaCO_3$. Phase boundaries from calcite I (CCI) to
670 calcite IV (CCIV), and calcite V, are labelled as M76-Mirwald (1976), and BS03-Bagdassarov and
671 Slutskii (2003). Transition curves from calcite to aragonite as experimentally investigated by L17-
672 Litasov et al. (2017), S01 - Suito et al. (2001), M76 - Mirwald (1976), and IW75-Irving and Wyllie
673 (1975), predicted by calorimetric measurements by R89-Redfern et al. (1989), and calculated with
674 thermodynamic database from HP11-Holland and Powell (2011), and HP02-Holland and Powell
675 (1998). Open diamonds represent experiments at 6 GPa by B03 - Buob (2003) where aragonite was
676 observed as the stable $CaCO_3$-polymorph. Open triangle and filled triangle represent experiments
677 by S14 - Shatskiy et al. (2014) where aragonite and melt, respectively, have been detected. Melting
678 was investigated by S18-Shatskiy et al. (2018), Li17-Li et al. (2017), IW75-Irving and Wyllie
679 (1975), and S01-Suito et al. (2001). The sub-oceanic ridge and ocean islands geotherms are from
680 Dasgupta and Hirschmann, 2010.

681

682 **Figure 2**

683 Secondary electron image of fibrous crystals of calcium carbonate (Run products CCMS1: 4.7 GPa-
684 1700 °C). These morphologies are interpreted as disequilibrium textures developed during rapid
685 cooling from a $CaCO_3$-liquid present at run conditions.

686

687 **Figure 3**

688 Experimental results and phase boundaries for the system $CaCO_3$, as predicted by employing
689 thermodynamic parameters from this study (solid line), HP11 database (dashed line), and HP02

690 update (dotted line). Results are compared with experimental data from IW75 (Irving and Wyllie,
691 1975), Li17 (Li et al., 2017) with "Pt sphere" (falling sphere) and ECM (electrical conductivity
692 measurements) experiments, B03 (Buob, 2003), S14 (Shatskiy et al., 2014), and S01 (Suito et al.,
693 2001). Filled green, open red, and filled violet symbols represent experimentally detected aragonite,
694 calcite V, and melt, respectively.

695

696 **Figure 4**

697 Unit cell volume of $CaCO_3$ vs. temperature data from this study at ambient pressure. The filled
698 circles represent the phase calcite - I. The open circles are phase calcite - IV and filled triangles are
699 disordered phase of calcite - V.

700

701 **Figure 5**

702 Isothermal compression curves for $CaCO_3$L at 1773 K (green) and 2073 K (red), determined from
703 this study (solid lines), and by MD data fitted with Birch-Murnaghan equation of state by
704 Vuilleumier et al. (2014) (dashed lines). The red/green dots with pressure error bars are obtained by
705 FPMD calculations (Vuilleumier et al., 2014) and the red/green dots with pressure and density error
706 bars are obtained with the radial distribution functions by Hudspeth et al., (2018).

707

708 **Figure 6**

709 Calculated pseudosections for carbonated eclogite *bulk* composition of OTBC, modified (K_2O-free)
710 after Hammouda (2003). The thermodynamic parameters for $CaCO_3$ are prov ided by: (a), this
711 study; (b), Holland and Powell (2011). Solid solution models here used are Cpx(JH), Sp(JH),
712 Pl(JH), and Grt(JH) proposed by Jennings and Holland (2015), F by Connolly and Trommsdorff

(1991), and oCcM(EF) (Mg-Fe-Ca carbonate solid solution) by Franzolin et al. (2011). Carbonatitic *solidus* (purple curve), and silicate *solidus* (green curve), were experimentally determined by Hammouda (2003). Crosses show all the experiments with aragonite from Hammouda (2003), and the diamond shows the experiment with aragonite in this P-T region from Kiseeva et al., (2013). Red contours represent calculated modal contents of aragonite (wt.%). Phase abbreviations are: cpx - clinopyroxene, pl - plagioclase, grt - garnet, ky - kyanite, sp - spinel, F - fluid, mg-cc - magnesio-calcite$_{s.s.}$, mst - magnesite, arag - aragonite, q - quartz, coe - coesite, stv - stishovite.

Figure 7

Calculated pseudosections for carbonated eclogite *bulk* composition of a) SLEC1 (Dasgupta et al., 2004), and b) EC1 (Yaxley and Brey, 2004), by employing the thermodynamic parameters for $CaCO_3$ retrieved from this study. *Bulk* compositions have been simplified by neglecting the TiO_2, MnO, Cr_2O_3, and K_2O components. Green *solidus*, and blue *solidus* curves are provided by Dasgupta et al. (2004), and Yaxley and Brey (2004), respectively. Red contours represent calculated modal contents of aragonite (wt.%). Phase abbreviations are: cpx - clinopyroxene, ol - olivine, grt - garnet, sp - spinel, mg-cc - magnesio-calcite$_{s.s.}$, cc-dol - calcio-dolomite$_{s.s}$, mst - magnesite, arag - aragonite.

Figure 8

Projected *bulk* compositions of reference carbonated eclogites, in a ternary $CaCO_3$-$MgCO_3$-$NaAlSi_2O_6$ compositional space: OTBC (Hammouda, 2003), SLEC1 (Dasgupta et al., 2004), GA1cc and Volga (Kiseeva et al., 2013), and EC1 (Yaxley and Brey, 2004). *Bulk* compositions

were projected from SiO_2 + TiO_2 + CO_2 + Fe↔Mg (exchange vector) + ternary garnet $(Mg_{0.5}Fe_{1.5}Ca_{1.0})Al_2Si_3O_{12}$.

Figure 9

$[La/Nb]_{norm.}$ versus $[La/Sm]_{norm.}$ diagram, normalized to the Primitive Mantle (PM) of Sun an McDonough (1989). Coloured diamonds refer to experimentally synthesized phases on carbonate sediments at 7.5 GPa - 900 °C (Brey et al., 2015): violet - aragonite, red - melt, blue - magnesite, green - garnet. Red, and orange circles represent Group I, and Group II close-to-primary kimberlite compositions, respectively (Becker and Le Roex, 2006). OIB and N-MORB compositions are from Sun and McDonough (1989), primitive arc andesites composition from Kelemen et al. (2003). A schematic representation is reported for coexisting phase assemblage in the experiments of Brey et al. (2015), on the basis of topologies discussed in Poli (2016).

Table 1

Experimental run conditions and run products in the pure $CaCO_3$ system. M - melt, Cc - calcite, Ara - aragonite.

Run	P (GPa)	T (°C)	Run time (hours)	Run products
CCMS1	4.7	1700	1.55	M
CCMS3	3.0	1650	2.6	M
CCMS4	3.8	1700	0.83	M
CCMS18	3.8	1500	24.17	Cc
CCMS19	4.7	1500	22.3	Ara
CCMS20	4.3	1500	17.5	Cc + Ara
CCMS21	3.3	1300	20	Cc
CCMS28	3.8	1300	27.42	Cc
CCMS30	4.2	1300	24.23	Ara
CCMS31	4.7	1650	2.0	Ara
CCMS34	6.0	1750	2.0	M

Table 2

Standard molar thermodynamic properties of Aragonite, Calcite V and $CaCO_3L$ at 298.15 K and 1 bar. G_0 - Gibbs free energy, H_0 - enthalpy, S_0 - entropy, V_0 - volume, Cp - heat capacity, α_0 - thermal expansivity, K_0 - bulk modulus, K′ - pressure derivative of the bulk modulus.

	G_0 (J)	H_0 (J)	S_0 (J/K)	V_0 (J/bar)	$C_{p,298.15}$ (J/K)	α_0 (1/K)	K_0 (bar)	K′
Aragonite	-1233820	-1207586	87.99	3.395	81.2	1.082E-4	689960	4.397
Calcite V	-1229812	-1199884	100.38	3.60	83.3	1.10E-4	725200	4.0
$CaCO_3L$	-1174842	-1139660	118.0	4.045	125.7	2.473E-4	78000	4.0

Fitted coefficients of C_p referred to the polynomial Eq. (7)

	a	b	c	d
Aragonite	137.906	0.023	-602802.8	-980.885
Calcite V	88.61	0.03945	-1094483.95	-81.726
$CaCO_3L$	117.071	0.01409	-12434.329	79.396

776 **Table 3**

777 *Bulk* compositions of reference carbonated eclogites expressed in wt.% oxides. OTBC, Hammouda
778 (2003), SLEC1, Dasgupta et al. (2004), EC1, Yaxley and Brey, (2004), GA1cc, Kiseeva et al.
779 (2013). #Mg is Mg/(Mg+Fe_T) molar ratio. #Ca is Ca/(Ca+Mg+Fe_T) molar ratio.

	OTBC	SLEC1	EC1	GA1cc
SiO_2	47.23	41.21	30.11	45.32
TiO_2	-	2.16	-	1.34
Al_2O_3	15.35	10.89	11.74	14.88
Cr_2O_3	-	0.09	-	-
FeO_T	8.93	12.83	10.05	8.85
MnO	-	0.12	-	0.15
MgO	6.24	12.87	12.44	7.15
CaO	14.77	13.09	19.41	14.24
Na_2O	2.91	1.63	0.87	3.14
K_2O	0.02	0.11	-	0.40
P_2O_5	-	-	-	0.14
CO_2	4.43	5.00	15.38	4.40
H_2O	0.12	-	-	-
Total	100.00	100.00	100.00	100.00
#Mg	0.555	0.641	0.688	0.590
#Ca	0.485	0.319	0.435	0.458

780

Figure1

Click here to download high resolution image

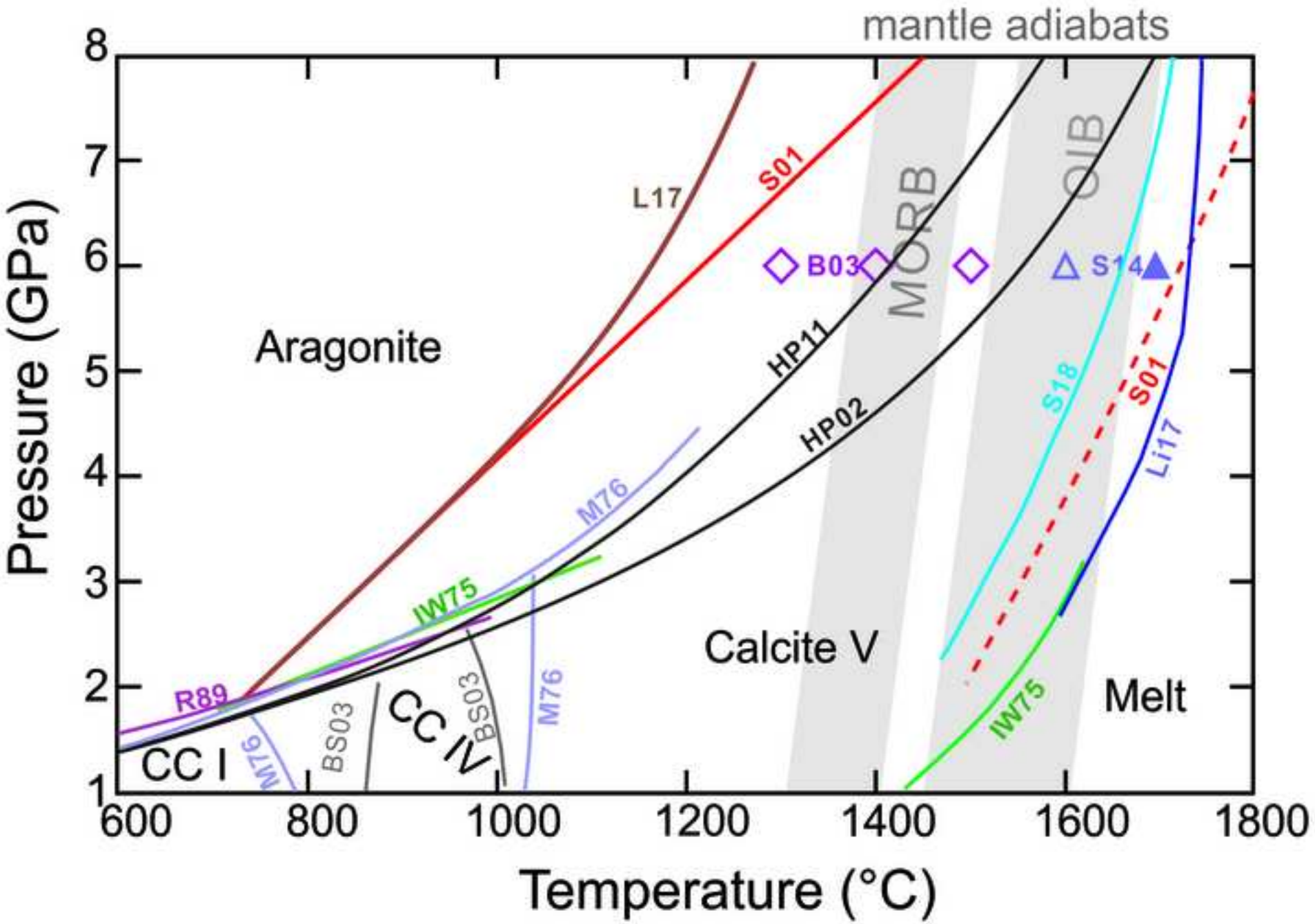

Figure2

Click here to download high resolution image

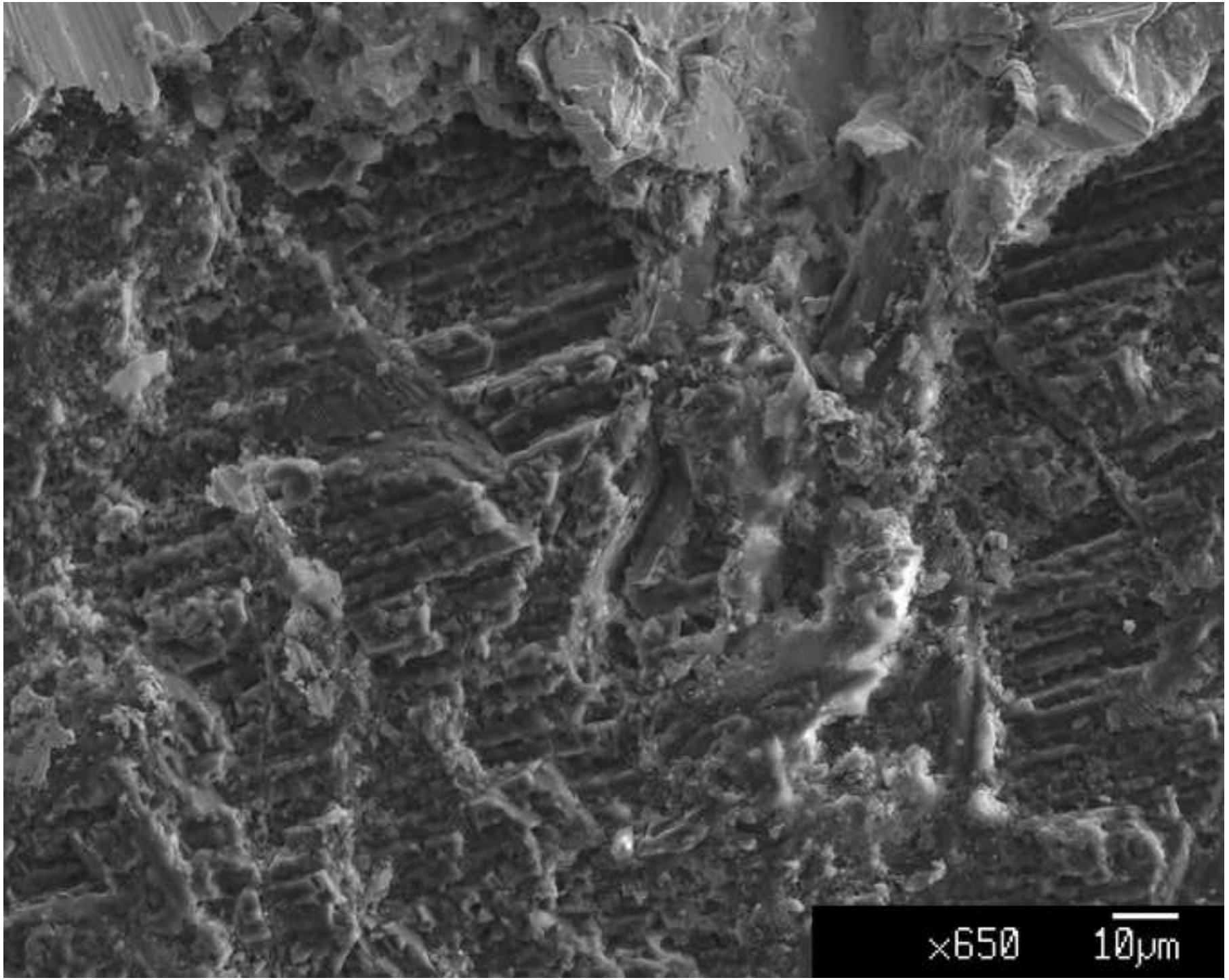

Figure3

Click here to download high resolution image

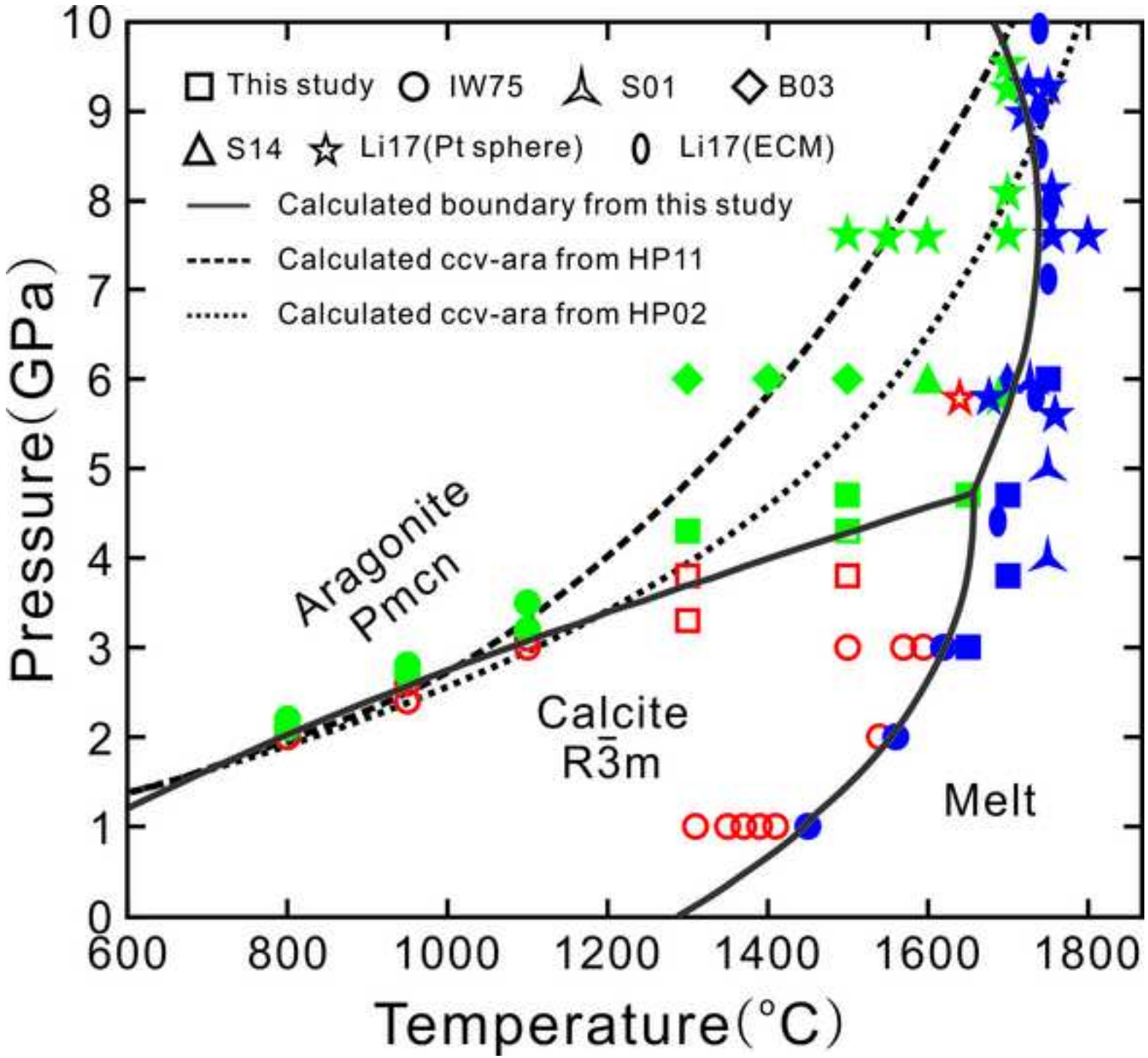

Figure4

Click here to download high resolution image

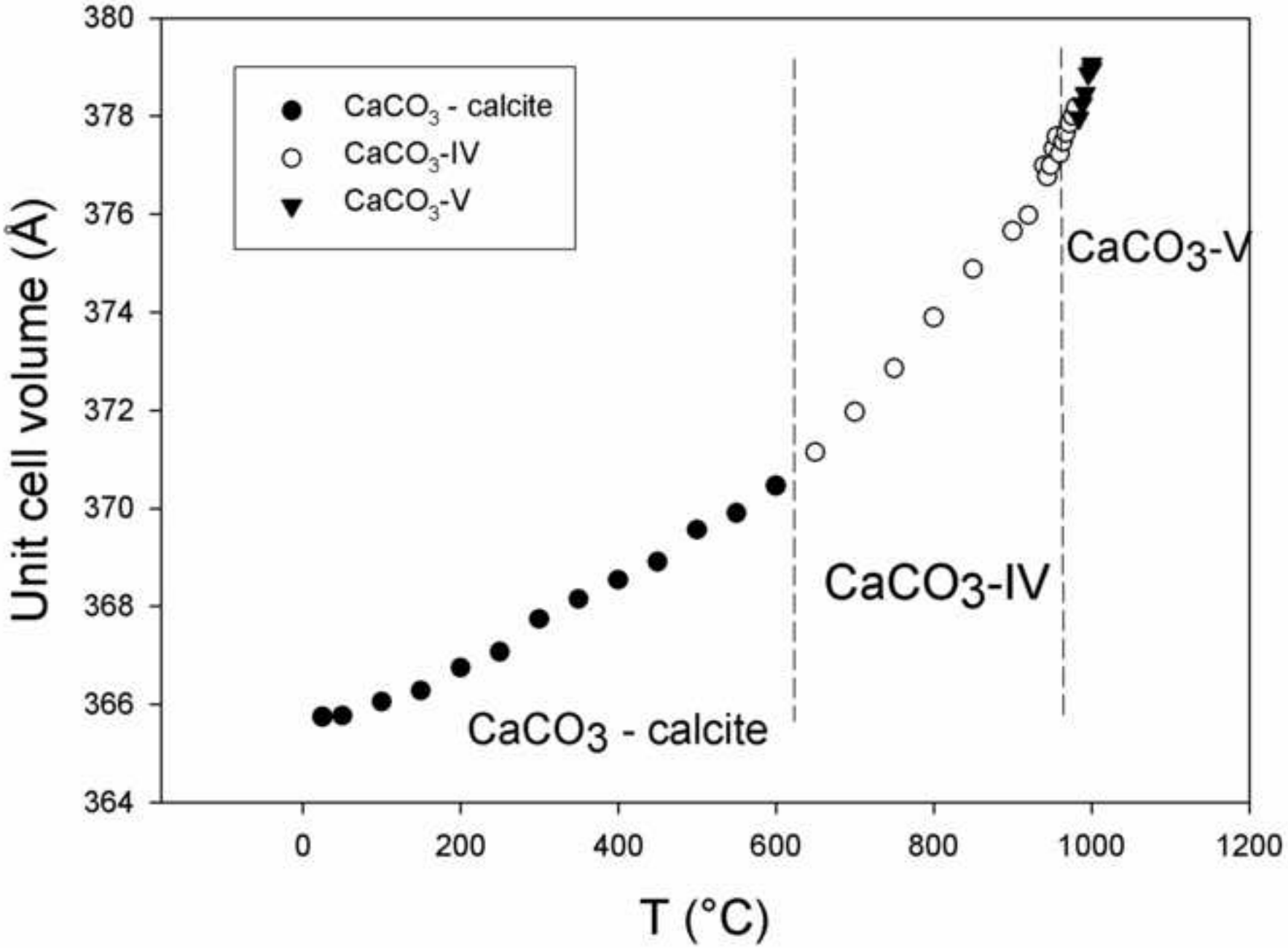

Figure5

Click here to download high resolution image

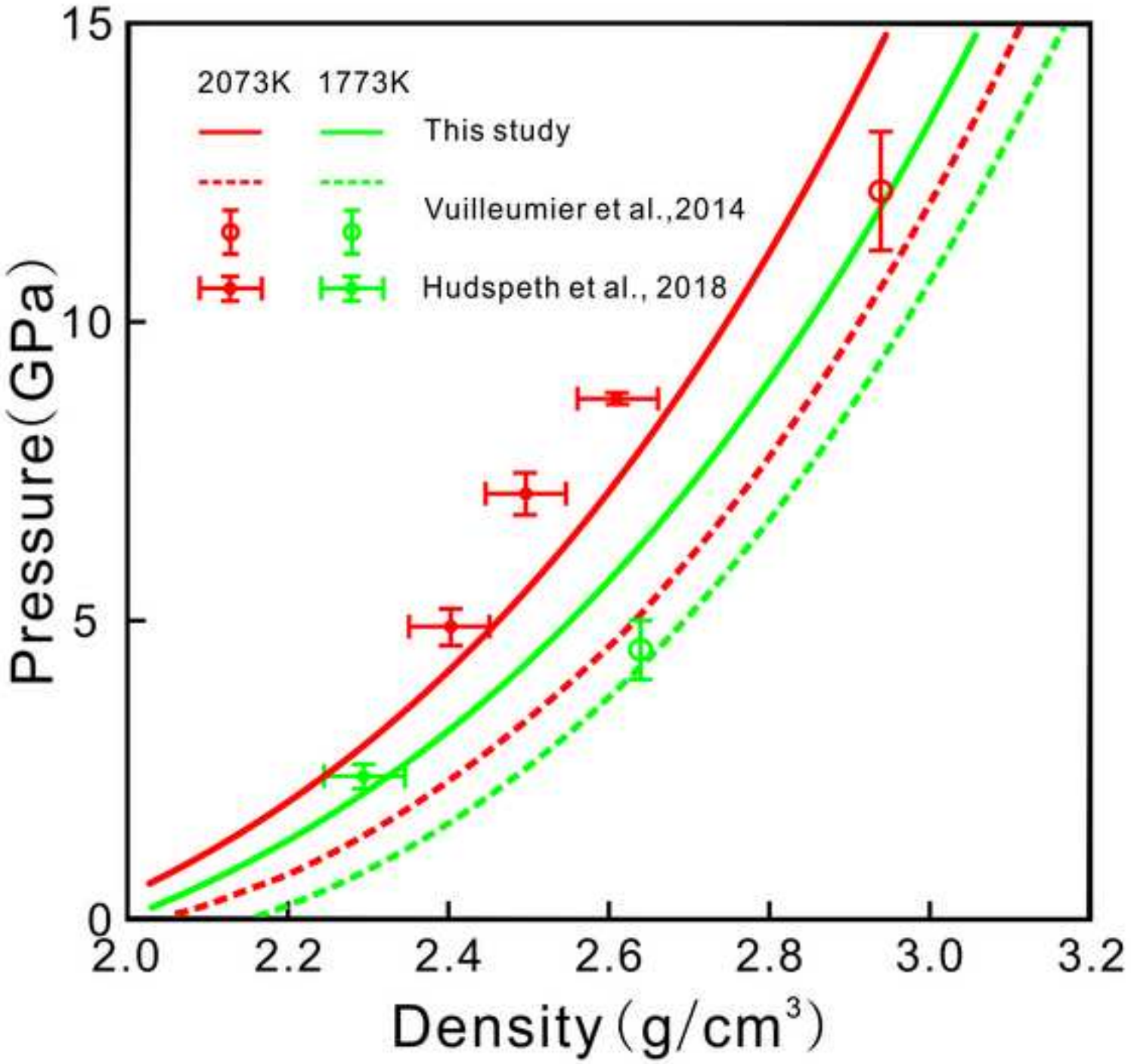

Figure6

Click here to download high resolution image

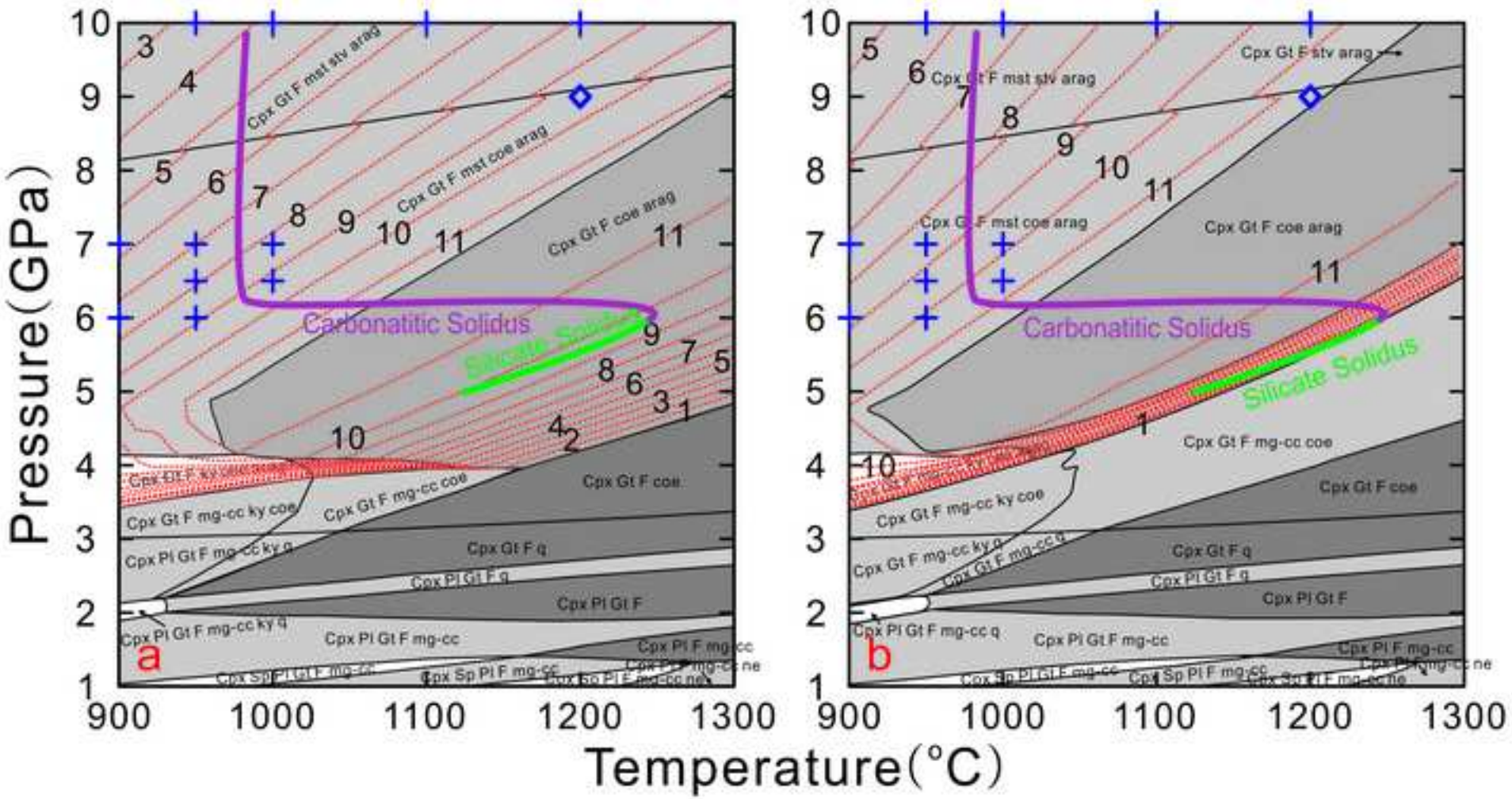

Figure7

Click here to download high resolution image

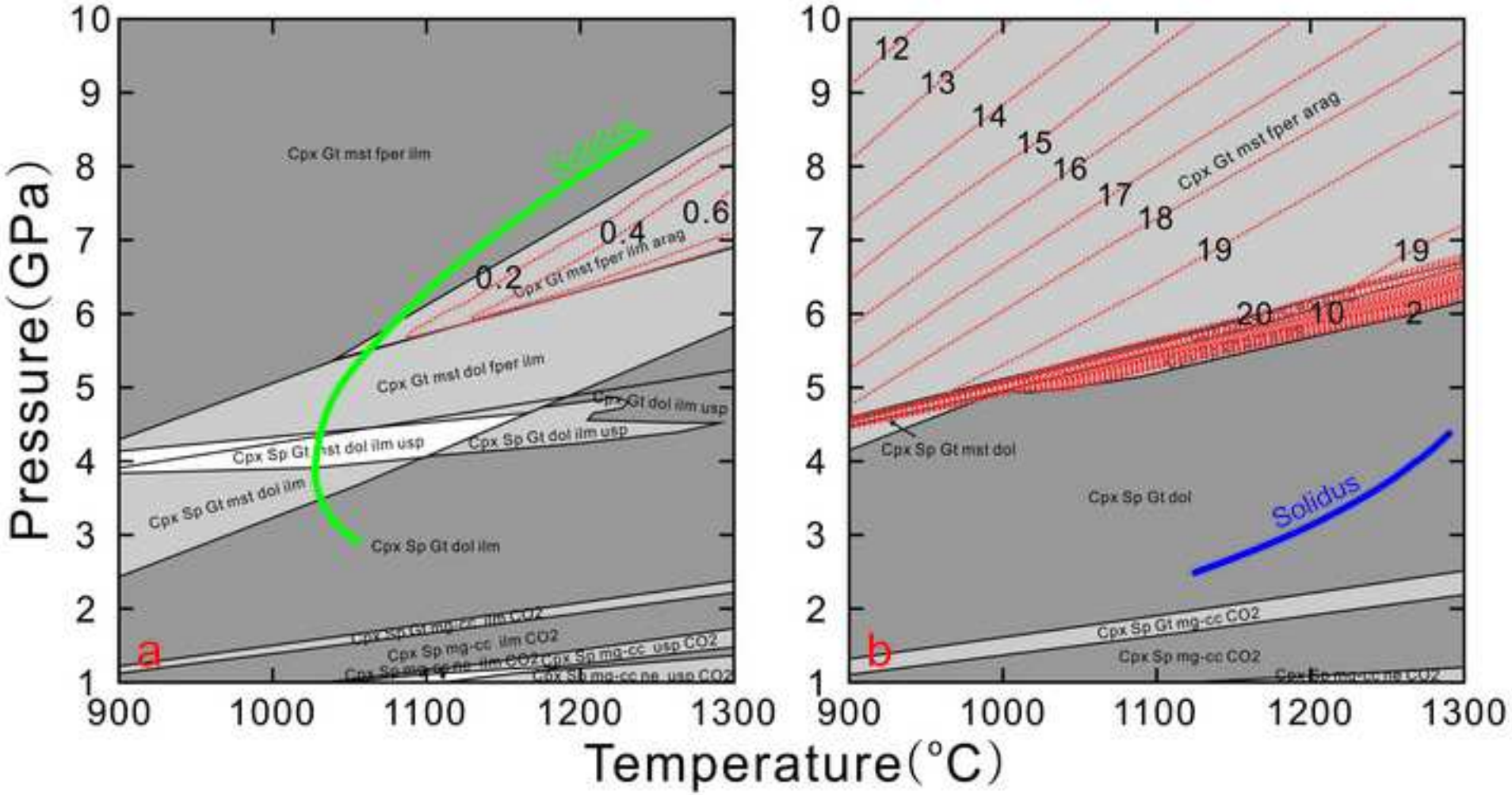

Figure8

Click here to download high resolution image

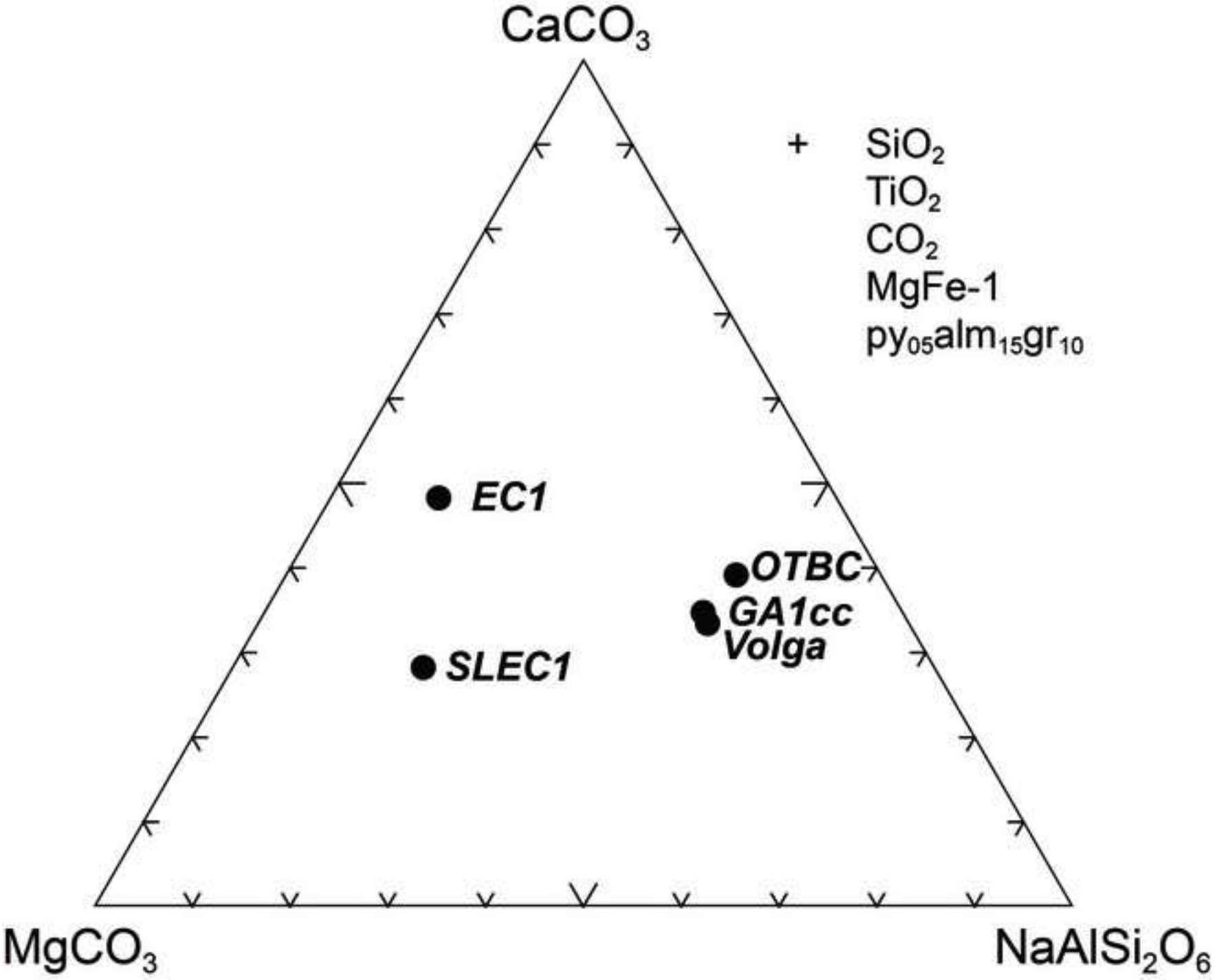

Figure9

Click here to download high resolution image

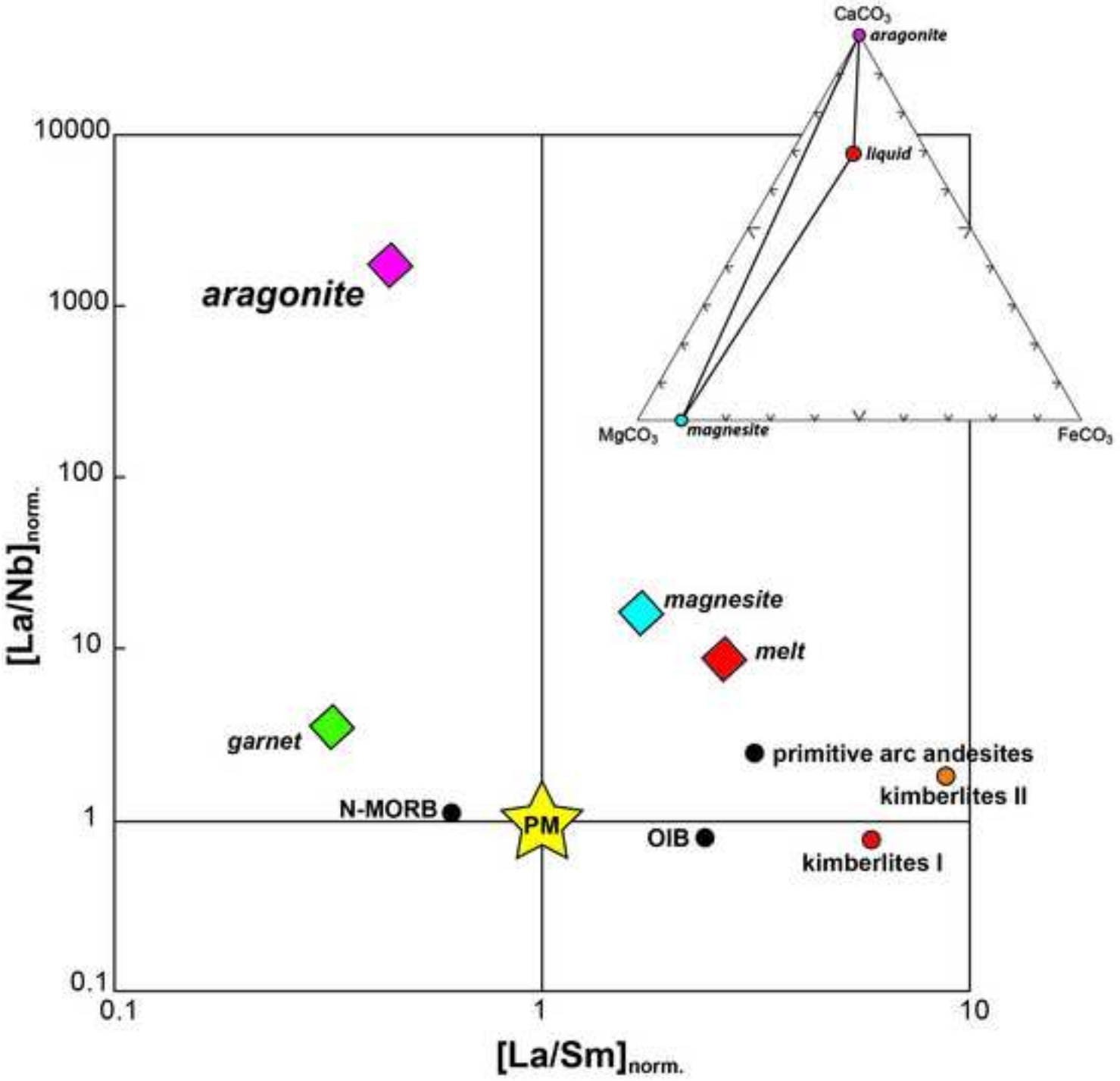

Supplementarydata_A

Click here to download Background dataset for online publication only: Supplementarydata_A.docx

Supplementarydata_B

Click here to download Background dataset for online publication only: Supplementarydata_B.docx